Morphology and Nonisothermal Crystallization of a Polyacetal/Poly(ε-caprolactone) Reactive Blend Prepared via a Chain-Transfer Reaction

Kuniaki Kawaguchi,[1] Hiroaki Nakao,[1] Eiji Masuda,[1] Yoshihisa Tajima[2]

[1]*Research and Development Center, Polyplastics Company, Limited, 973 Miyajima, Fuji, Shizuoka, 416-8533 Japan*
[2]*Technical Solution Center, Polyplastics Company, Limited, 973 Miyajima, Fuji, Shizuoka, 416-8533 Japan*

Received 19 July 2007; accepted 1 August 2007
DOI 10.1002/app.27144
Published online 9 October 2007 in Wiley InterScience (www.interscience.wiley.com).

ABSTRACT: A polyacetal (POM)/poly(ε-caprolactone) (PCL) reactive blend prepared via a chain-transfer reaction was investigated with respect to its morphology and nonisothermal crystallization, and the results were compared with those of a simple POM/PCL blend. The reactive blend had a microscopically phase-separated morphology in which the diameter of the PCL microphase was below 100 nm, and it clearly yielded ring-banded spherulites, whereas between the two blends, there were no significant differences in the diameters and polygonal edges of the spherulites and in the long period of the POM phases. The PCL part of the reactive blend crystallized within the confined microspace with about 10% lower crystallinity than that of the corresponding simple blend. A lower Avrami exponent and crystallization rate parameter of the PCL part were observed in the primary crystallization process of the reactive blend. In contrast, the crystallinity of the POM component and the nonisothermal crystallization kinetic parameters of the POM part showed no noticeable differences between the two blends at any given cooling rate. © 2007 Wiley Periodicals, Inc. J Appl Polym Sci 107: 1269–1279, 2008

Key words: crystallization; differential scanning calorimetry (DSC); morphology; spherulites

INTRODUCTION

Polyacetal [alternatively called acetal resin or polyoxymethylene (POM)] is a major engineering thermoplastic of industrial importance that has been used extensively for versatile applications in automotive, electrical, and electronics industries, among others, because of its well-balanced mechanical properties, abrasion wear-resistance properties, and good processability. To improve the performance of conventional POM, several studies[1–5] have been focused on the synthesis and properties of modified POMs prepared via a chain-transfer reaction in the presence of a chain-transfer agent such as an oligomeric or polymeric compound. Masamoto et al.[1] demonstrated that block copolymers comprising POM and a small fraction of polyethylene could be obtained by the polymerization of 1,3,5-trioxane (TOX) with a formal compound with an alkyl chain. They investigated the morphology of the copolymer on the basis of small-angle X-ray scattering (SAXS) measurements in a molten state and reported that the crystallizable polyethylene part exhibited microphase separation. Matsuzaki et al.[2] reported that a POM block copolymer derived by the polymerization of formaldehyde in the presence of an alcoholic compound having both alkyl and ether chains possessed good lubrication properties. They also reported that formaldehyde was polymerized in the presence of modified ethylene–propylene rubber (EPR) as a chain-transfer agent, and the resultant POM-grafted EPR showed improved toughness.[2]

Preparation of modified POMs comprising POM and an aliphatic polyester have been reported in the patent literature.[3–5] However, the morphology and crystallization, which are the most important characteristics in determining the mechanical properties, have not yet been investigated for these modified POMs. In this case, these characteristics are expected to work in different and complicated manners because of the mutual influence of the POM and aliphatic polyester.[1,6–12] α,ω-Dihydroxy poly(ε-caprolactone) (PCL) is one of the useful chain-transfer agents and is commercially available for practical use as a biodegradable plastic. In this study, a reactive POM/PCL blend was prepared via cationic bulk polymerization of TOX with 1,3-dioxolane (DOX) in the presence of PCL as a chain-transfer agent, and its morphology and crystallization are discussed in comparison with those of a simple POM/PCL blend to clarify the mutual influence of the POM and PCL parts. The morphology of the blends was investigated with scanning electron microscopy (SEM),

Correspondence to: K. Kawaguchi (kuniaki.kawaguchi@polyplastics.com).

Journal of Applied Polymer Science, Vol. 107, 1269–1279 (2008)

transmission electron microscopy (TEM), wide-angle X-ray diffraction (WAXD), SAXS, and polarized light microscopy (PLM). To investigate the crystallization behavior and kinetics of both parts in the blends, nonisothermal crystallization analysis was performed at different cooling rates by differential scanning calorimetry (DSC).

EXPERIMENTAL

Preparation

To prepare the reactive POM/PCL blend, cationic bulk polymerization of TOX with DOX (4.0 mol %) was performed in the presence of PCL (5.0 wt %) with boron trifluoride as a catalyst. TOX and DOX were supplied by Polyplastics (Shizuoka, Japan). PCL was supplied by Daicel Chemical Industries (Tokyo, Japan) and was dried in a vacuum oven. The weight-average molecular weight (M_w) of the initial PCL prepolymer (neat polymer) was 3.80×10^4 g/mol. A continuous-type reactor was used for the polymerization, and the reactor temperature was maintained at 80°C. For thermal and chemical stability of the sample, DOX was used for the occasional insertion of a carbon-to-carbon linkage in the polymer chain. Before the polymerization, PCL was predissolved in TOX, and the monomer mixtures were fed into the reactor. A small amount of dimethoxymethane was used as a chain-transfer agent for adjusting the molecular weight. The discharged raw sample from the reactor was poured into a triethylamine aqueous solution at room temperature to deactivate the catalyst. The resulting raw sample was posttreated in a molten state (at 200°C) to remove unstable hemiformal fractions[13] and was formed into pellets. Additionally, to prepare a simple POM/PCL blend for reference, a neat POM was similarly prepared, except that the polymerization took place in the absence of PCL, and the neat POM that resulted was blended with 10 wt % neat PCL in a melt mixer at 200°C.

Characterization

To analyze the composition of DOX and PCL in the samples, ^{1}H-NMR spectra were obtained at 45°C on a Bruker Avance 400 spectrometer (Switzerland) operated at 400 MHz. The samples were dissolved in 1,1,1,3,3,3-hexafluoro-2-propanol-d_2, and the deuterated solvent was used to provide an internal lock signal. The molar composition of DOX was determined by ^{1}H-NMR with the following equation:

$$[\mathrm{DOX}] = \{(A_{\mathrm{C2H4O}}/2)/[(A_{\mathrm{CH2O}} + A_{CH2OC2H4O} - A_{\mathrm{C2H4O}}/2)/3 + A_{\mathrm{C2H4O}}/2]\} \times 100 \quad (1)$$

where [DOX] is the molar percentage of DOX and A_x represents the corresponding peak area. The weight composition of PCL was determined with the following equation:

$$[\mathrm{PCL}] = \{114.14 \times A_{\mathrm{CH2}}/[114.14 \times A_{\mathrm{CH2}} + 44.05 \times A_{\mathrm{C2H4O}}/2 + 30.03 \times (A_{\mathrm{CH2O}} + A_{CH2OC2H4O})]\} \times 100 \quad (2)$$

where [PCL] is the weight percentage of PCL and A_{CH2} represents the peak area of PCL methylene protons observed at 2.4 ppm in the chemical shift.

Size exclusion chromatography (SEC) was performed at 40°C on a Tosoh (Japan) HLC-8220GPC instrument equipped with polystyrene gel columns with 1,1,1,3,3,3-hexafluoro-2-propanol as an eluent containing a small amount of trifluoroacetic acid sodium salt. The calibration master curve for the molecular weight against the elution time was determined with poly(methyl methacrylate) with a narrow molecular distribution as a standard. M_w was calculated from this standard curve.

Morphological investigation

SEM observations were performed on a Hitachi (Japan) S-4700 at room temperature. The samples were cryogenically fractured after immersion in liquid nitrogen and etched with chloroform for 1 h at room temperature to etch the PCL portion selectively. Thereafter, they were ion-sputtered with platinum and palladium *in vacuo*. The phase morphology of the samples was investigated with an acceleration voltage of 3 kV.

The morphology of the thin section of the specimens was investigated on a Hitachi H-7650 transmission electron microscope. The polymeric pellets were held at 200°C for 3 min under 20 MPa, rapidly cooled to crystallize in a water bath, and then dried in a vacuum oven. Afterward, the compression-molded specimens, 1 mm thick, were stained with ruthenium tetroxide (RuO_4) to improve contrast, and the specimens were cut with an ultramicrotome.

WAXD was performed on a Rigaku (Japan) RINT2500HL with Cu Kα radiation at an accelerating voltage of 40 kV and a current of 100 mA. The compression-molded specimens, 1 mm thick, were used for the analysis at room temperature.

SAXS was performed on a Rigaku NANO-Viewer IP with Cu Kα radiation at an accelerating voltage of 40 kV and a current of 20 mA. The compression-molded specimens, 1 mm thick, were used for the analysis at room temperature.

PLM observation was performed with an Olympus (Japan) BX51. The specimens were prepared by the direct pressing of each sample once between two glass slides without a spacer in a molten state. Thereafter,

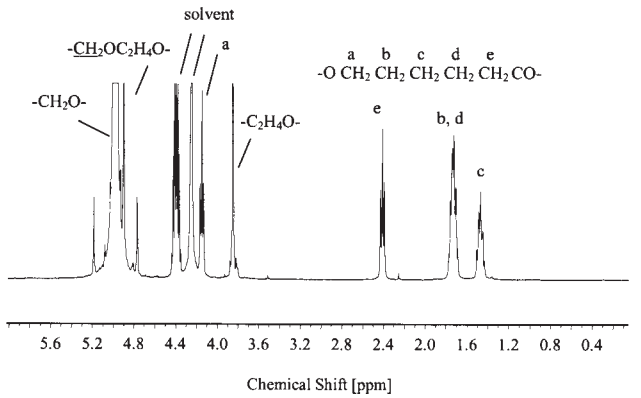

Figure 1 ^{1}H-NMR spectrum of the reactive POM/PCL blend.

the specimens were heated to 200°C, kept for 1 min, and then cooled to room temperature at 5 or 40°C/min. The thickness of the specimens was controlled to about 20 μm, and the crystalline morphology of the specimens was investigated at room temperature.

DSC measurements

DSC measurements were performed with a TA Instruments (USA) Q1000 equipped with a rapid cooling system. Approximately 5-mg samples were used for the measurements. All experiments were performed under a nitrogen atmosphere, and the samples were encapsulated in aluminum pans. In many cases, polymer materials for practical processing are well used under nonisothermal crystallization conditions. For that reason, nonisothermal crystallization analysis is an important analytical category. Therefore, in this study, the experiments were performed under nonisothermal conditions. For analysis of the nonisothermal crystallization, the samples were heated to 200°C and kept for 1 min to remove any thermal history and were then cooled to −20°C at different cooling rates of 5, 10, 20, and 40°C/min.

RESULTS AND DISCUSSION

Characterization

The characteristics of the samples were investigated with ^{1}H-NMR and SEC. Figure 1 shows the ^{1}H-NMR spectrum of the reactive POM/PCL blend. The signals assigned to the PCL component were clearly detected in the spectrum. The PCL and DOX contents for the samples were calculated from the area of each characteristic peak on the basis of the NMR peak assignments [eqs. (1) and (2)], and the results are given in Table I. The DOX content (molar composition) of the reactive blend and the neat POM was 3.7 and 3.9 mol %, respectively. The reactive blend had a 7.3 wt % concentration of the PCL component (weight composition), which was about 50% higher than the fed amount of PCL. This phenomenon should be attributed to the fact that the residual TOX, DOX, and unstable hemiformal fractions[13] were lost during the polymerization and the posttreatment, whereas almost all of the PCL component reacted and remained in the reactive blend during this processing. During cationic ring-opening polymerization of TOX and DOX, cationic active sites undergo chain transfer[14] with a hydroxyl end group in the PCL, and the PCL segments are chemically linked to the POM segments (Scheme 1). The NMR spectrum exhibited no signal of blocked DOX segments, indicating that DOX was randomly incorporated into the polymer backbone because of an intermolecular transacetalization reaction.[15] In this case, the attack of a carbonium cation on an intermolecular oxygen results in the formation of another carbonium cation and a polymer and in the rearrangement of the polymer sequence. The PCL composition of the simple POM/PCL blend was adjusted to 10.0 wt %, which was a somewhat higher value than that of the reactive blend. The values of M_w of the samples obtained from SEC analysis are listed in Table I. The reactive blend had an M_w value of 1.15×10^5, which was nearly equal to the M_w value of the simple blend.

TABLE I
Characteristics of the Blends and Neat Polymers

	DOX (mol %)[a]	PCL (wt %)[b]	M_w (g/mol)
Reactive POM/PCL blend	3.7	7.3	1.15×10^5
Simple POM/PCL blend	3.9	10.0	1.10×10^5
POM	3.9	—	1.38×10^5
PCL	—	100	3.80×10^4

[a] Calculated with eq. (1).
[b] Calculated with eq. (2).

Morphological investigation

Figure 2 shows SEM micrographs of the simple POM/PCL blend and the reactive POM/PCL blend

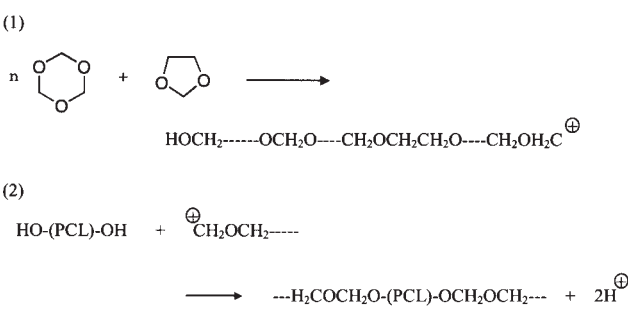

Scheme 1 Polymerization of TOX and DOX in the presence of PCL: (1) cationic ring-opening copolymerization and (2) chain transfer to the hydroxyl end group.

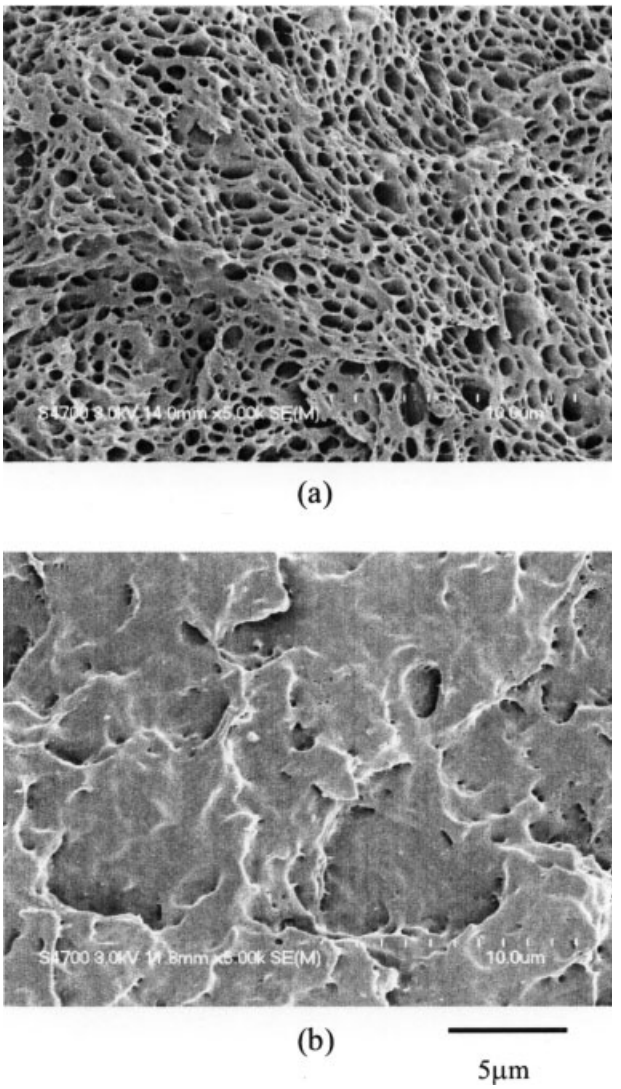

Figure 2 SEM micrographs of cryogenically fractured surfaces: (a) simple POM/PCL blend and (b) reactive POM/PCL blend. The samples were cryogenically fractured after immersion in liquid nitrogen and etched with chloroform for 1 h at room temperature.

after etching with chloroform. The simple blend had a two-phase morphology and macroscopically dispersed PCL phases as sunken cavities, whose diameters ranged from about 0.5 to 1.5 μm, distributed in a POM matrix phase. In contrast, there were no clear PCL phases on the fractured surface of the reactive blend, and its overall morphology was indistinct. To investigate the phase morphology of the reactive POM/PCL blend, TEM images were taken of thin sections of the compression-molded specimens, which were rapidly cooled to room temperature from a molten state, as shown in Figure 3. The PCL phase, preferentially stained with RuO_4, appeared as darker particles; the micrographs clearly show a microscopically phase-separated morphology. In addition, the POM phase was partially stained with RuO_4, and the radial pattern arising from the crystallites partially appeared as darker regions. Compared to the simple blend, the PCL phase was still distributed in the POM phase, but the particle size decreased significantly; the diameter of the discrete PCL microdomain was below 100 nm, and this

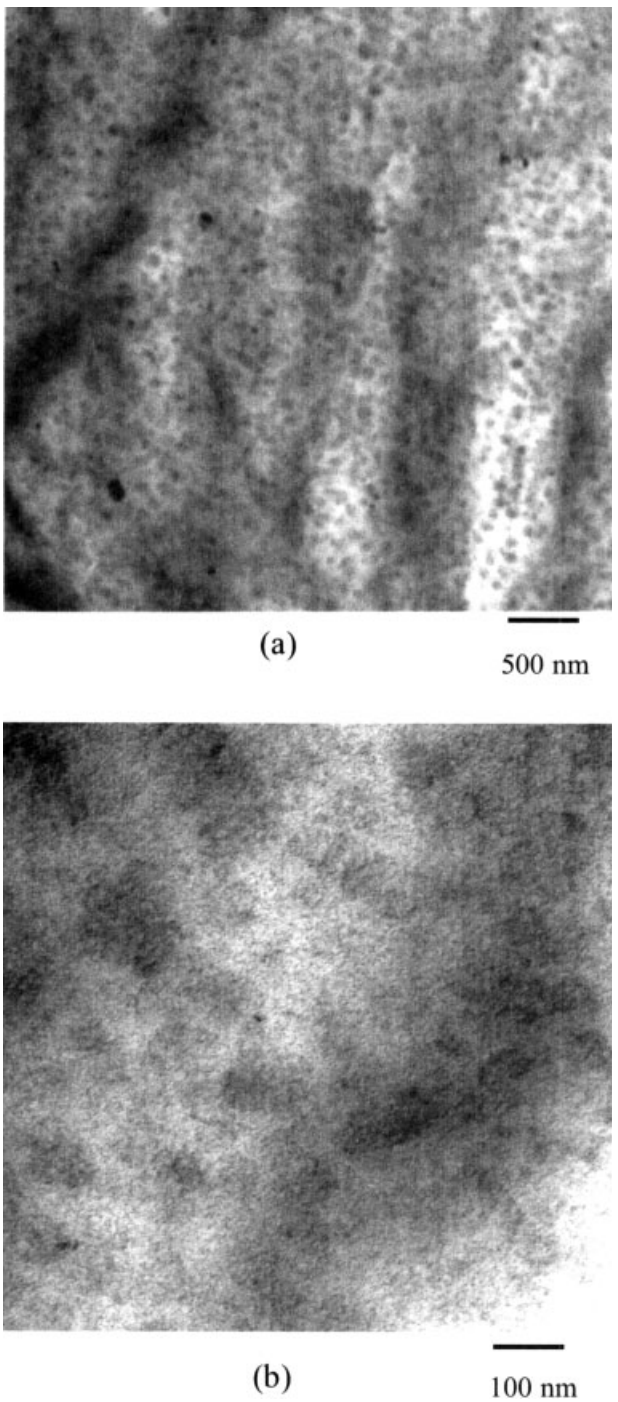

Figure 3 TEM micrographs of a thin section of a specimen rapidly cooled to room temperature from 200°C: (a) reactive POM/PCL blend and (b) magnified photograph of the same blend. The PCL phase, preferentially stained with RuO_4, appears as darker particles.

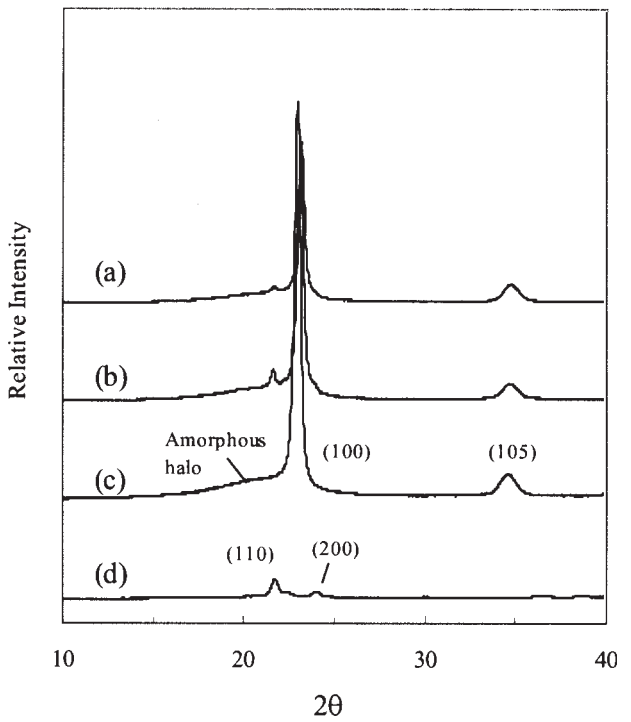

Figure 4 WAXD patterns against diffraction angle 2θ: (a) reactive POM/PCL blend, (b) simple POM/PCL blend, (c) neat POM, and (d) neat PCL.

could not be achieved through simple blending. The results demonstrate that the PCL part is well dispersed in the reactive blend, but strong segregation occurs between the POM and PCL segments and accommodates the phase separation with the spherical microdomain. Figure 3 also shows that the individual microdomain was evenly distributed in the reactive blend, but the higher order lattice of the microdomain was poorly defined in the TEM micrographs.

Figure 4 shows WAXD profiles of the reactive POM/PCL blend, the simple POM/PCL blend, and the neat polymers (the compression-molded specimens). The curves have been displaced along the ordinate for better visualization. The diffraction peaks of (100) and (105) for the neat POM[16] and those of (110) and (200) for the neat PCL[17] were detected. The reactive blend and the simple blend substantially showed the same diffraction with the major POM component and the minor PCL component. The WAXD results mean that there is no eutectic crystal or mixed crystal consisting of both POM and PCL chains, and the POM and PCL crystals independently exist in both blends.[6] The results also indicate that the PCL part can crystallize within the confined microspace in the reactive POM/PCL blend. Figure 5 shows the SAXS profiles of the reactive POM/PCL blend, the simple POM/PCL blend, and the neat polymers (the compression-molded specimens). The Lorenz-corrected scattering intensity, $I(q)q^2$, was plotted as a function of the magnitude of the scattering vector, q, which was defined as follows:

$$q = (4\pi/\lambda)\sin\theta \tag{3}$$

where λ and θ are the wavelength of the X-ray (0.15418 nm) and half of the scattering angle, respectively. The curves have been displaced along the ordinate for better visualization. The SAXS peak arising from the long period, namely, the total lamellar spacing consisting of the crystalline and amorphous phases, was clearly observed in each profile. The neat POM had a higher peak position (q^*) of the SAXS peak than the neat PCL. The long period, $d = 2\pi/q^*$ by Bragg's equation, for the neat POM and the neat PCL was calculated to be 14.7 and 16.9 nm, respectively. There were no significant differences in the long periods of the POM phases between the reactive blend (15.1 nm) and the simple blend (14.7 nm), and both peak positions were nearly equal to that of the neat POM. No clear SAXS peak arising from the long period of the PCL phases was observed in either the reactive blend or the simple blend because the position of the minor PCL peak might be close to the POM peak.

The POM crystalline morphology was investigated by PLM with thin specimens, which were cooled to room temperature from 200°C at 5 or 40°C/min. PLM micrographs of the reactive POM/PCL blend and the simple POM/PCL blend are presented in Figure 6. The reactive blend clearly formed the ring-banded spherulite morphology, in which a Maltese cross pattern and negative birefringence faintly appeared at each cooling rate, as shown in Figure 6(a,b). It is known that radial banding arises from cooperative twisting of the crystalline lamella during

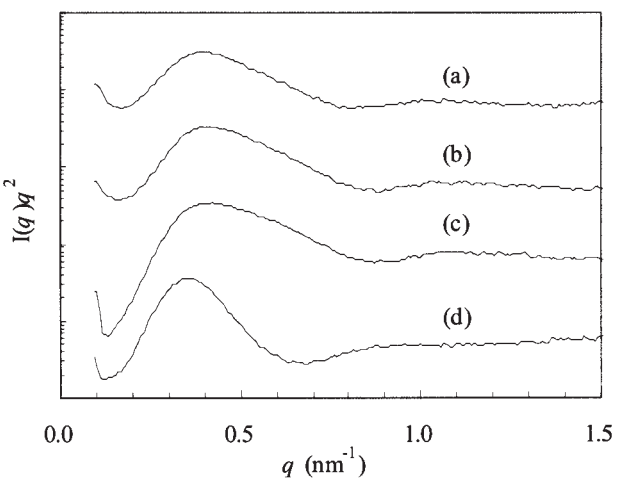

Figure 5 Lorenz-corrected SAXS intensity versus q: (a) reactive POM/PCL blend, (b) simple POM/PCL blend, (c) neat POM, and (d) neat PCL.

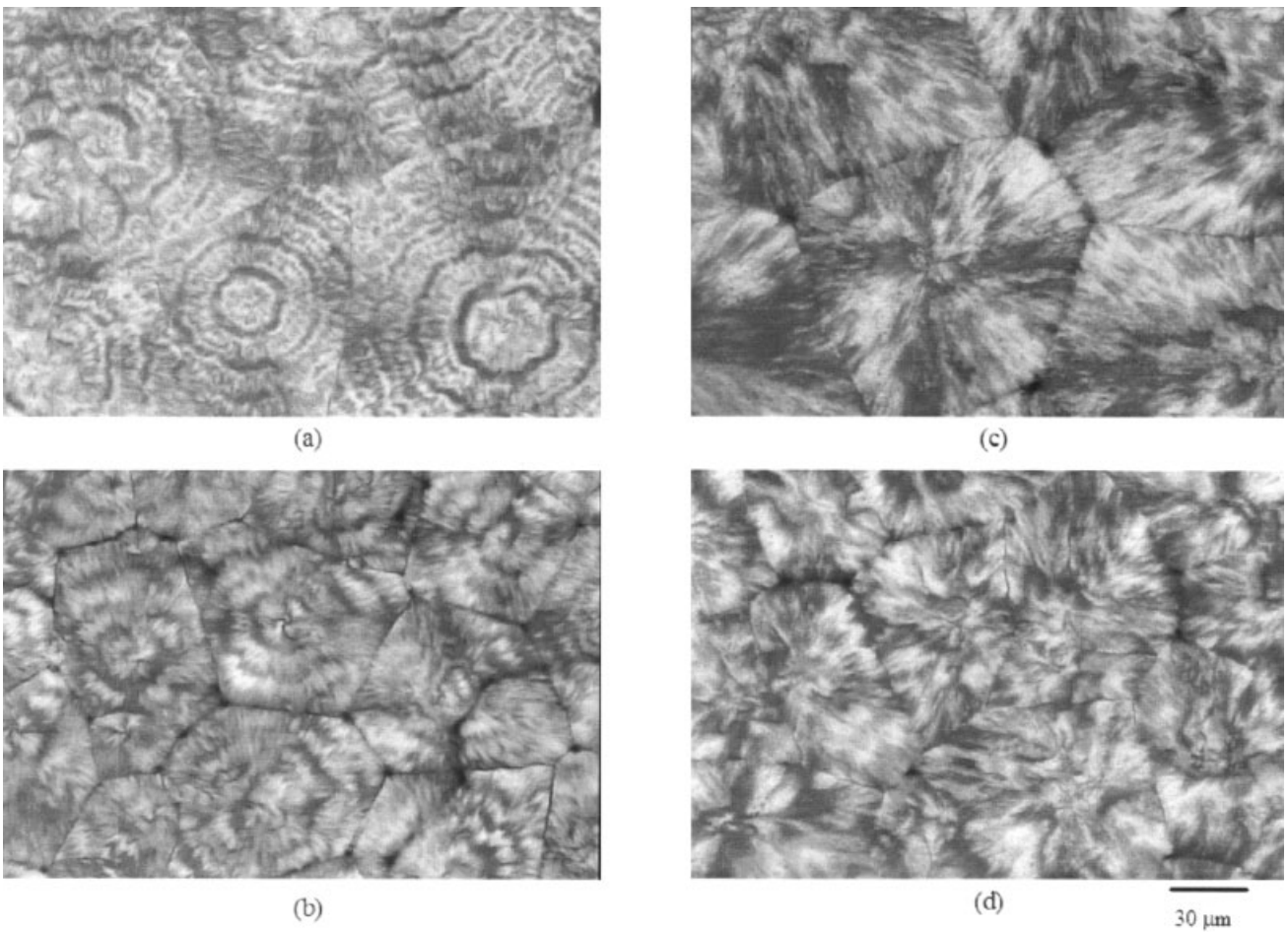

Figure 6 PLM micrographs of specimens cooled to room temperature from 200°C at different cooling rates: (a) reactive POM/PCL blend (5°C/min), (b) reactive POM/PCL blend (40°C/min), (c) simple POM/PCL blend (5°C/min), and (d) simple POM/PCL blend (40°C/min).

spherulitic growth and that the axial rotation of the lamella is caused by surface stresses.[18] The mechanism through which this structure is generated in the reactive blend can be attributed to the influence of the PCL microdomain on the cooperative twisting of the crystalline lamella of the POM component. The ring periodicity of the specimen whose cooling rate was 5°C/min was found to be longer than that of the corresponding one at 40°C/min, and this indicated that the twisting proceeds at a longer ring distance at a lower cooling rate. The diameter of the spherulites decreased with an increase in the cooling rate because of the combined temperature dependence of nucleation and spherulitic growth and was in a range from about 50 to 100 μm at 5°C/min and from about 30 to 80 μm at 40°C/min. It is conceivable that at a faster cooling rate, that is, 40°C/min, crystalline nuclei are activated at a lower temperature. As a result, comparatively smaller spherulites are yielded in the reactive blend. In contrast, the simple blend exhibited no ring-banded spherulitic texture, with the faint appearance of a Maltese cross pattern and negative birefringence, as shown in Figure 6(c,d). This spherulite morphology is nearly comparable to the distinct spherulites generally observed in neat POM, implying that the macroscopically dispersed PCL phase had little or no influence on the distortion of the crystallites within the POM spherulites. Such a series of morphological changes indicates that the POM spherulitic texture is very sensitive to differences in polymer architecture. The diameter of the spherulites of the simple blend grew shorter as the cooling rate increased, and this was similar to that of the corresponding reactive blend. According to qualitative comparisons of Figure 6(a,c) and Figure 6(b,d), there were no significant differences in the diameters and polygonal edges of the spherulites of the reactive blend and the simple blend at the same cooling rate.

Nonisothermal crystallization behavior

To investigate the nonisothermal crystallization behavior of the reactive POM/PCL blend and the

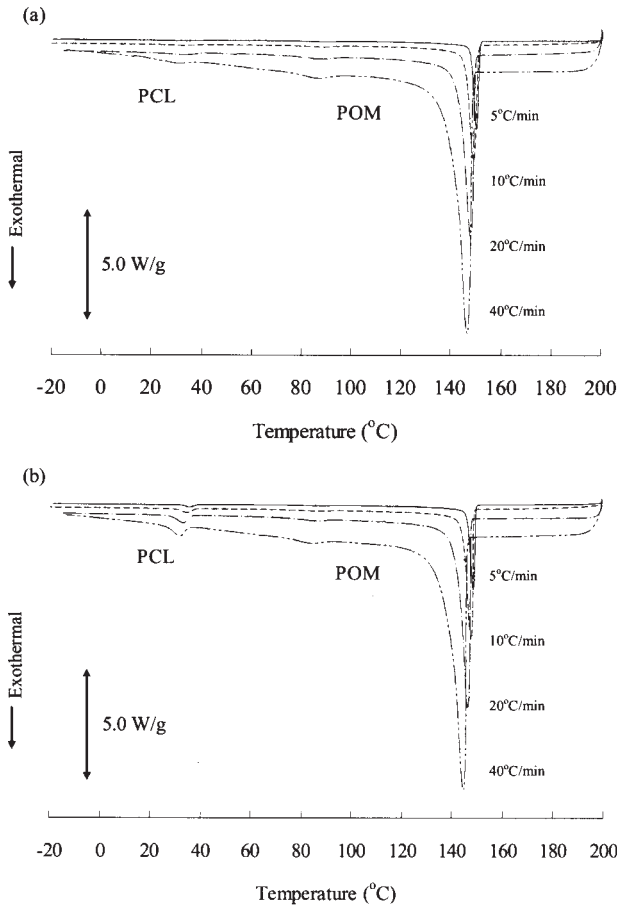

Figure 7 DSC crystallization thermograms: (a) reactive POM/PCL blend and (b) simple POM/PCL blend.

simple POM/PCL blend, DSC measurements were performed at each cooling rate, as shown in Figure 7. The DSC thermograms of the reactive blend [Fig. 7(a)] showed two crystallization peaks corresponding to the crystallization of the PCL and POM segments, indicating that the PCL part could crystallize within the confined microspace. The crystallization peak temperature (T_c), at which the crystallization rate was maximum, was measured at each cooling rate. In addition, the entire crystalline region was evaluated by its crystallinity (X_c), which was defined as follows for both the POM and PCL components:

$$X_c(\%) = [(\Delta H_c/W)/\Delta H^0] \times 100 \quad (4)$$

where ΔH_c is the measured crystallization enthalpy per unit gram of the blends, ΔH^0 is the enthalpy of fusion per unit gram for the 100% crystalline polymer, and W is the weight fraction. With respect to both the 100% crystalline POM[19] and PCL,[20] ΔH^0 are assumed to be 248.3 and 135.4 J/g, respectively. Table II shows the results of DSC measurements. The crystallization peak temperature of the PCL component ($T_{c\mathrm{PCL}}$) gradually shifted to a lower temperature region as the cooling rates increased from 5 to 40°C/min, indicating that a supercooling degree of crystallizing increased during this course. $T_{c\mathrm{PCL}}$ of the reactive POM/PCL blend appeared to be slightly lower than that of the simple blend. The crystallinity of the PCL component ($X_{c\mathrm{PCL}}$) of both blends [eq. (4)] gradually decreased as the cooling rate increased, indicating that the cooling rate affected $X_{c\mathrm{PCL}}$ under a nonisothermal process. The reactive blend had an approximately 10% lower vale of $X_{c\mathrm{PCL}}$ in comparison with the simple blend at each cooling rate. Similar conclusions about the reduction of the crystallinity of a minor block in block copolymers were reached by Xu et al.[10] and Gan et al.[11] The experimental results indicate that the major POM part in the reactive blend severely interferes with the crystallization of the minor PCL part, namely, the growth of the PCL crystallite, and eventually lowers $X_{c\mathrm{PCL}}$ within the confined microspace.

Similar to $T_{c\mathrm{PCL}}$, the crystallization peak temperature of the POM component ($T_{c\mathrm{POM}}$) gradually shifted to a lower temperature region with an increased cooling rate. The fact that $T_{c\mathrm{POM}}$ of the reactive blend was slightly higher than that of the simple blend is attributed to the slight difference in the DOX content in the POM component of both blends. The crystallinity of the POM component ($X_{c\mathrm{POM}}$) of the blends [eq. (4)], which was significantly higher

TABLE II
Nonisothermal Crystallization Parameters

	Cooling rate (°C/min)	PCL part			POM part		
		$T_{c\mathrm{PCL}}$ (°C)	$\Delta H_{c\mathrm{PCL}}$ (J/g)	$X_{c\mathrm{PCL}}$ (%)[a]	$T_{c\mathrm{POM}}$ (°C)	$\Delta H_{c\mathrm{POM}}$ (J/g)	$X_{c\mathrm{POM}}$ (%)[a]
Reactive POM/PCL blend	5	33.8	3.52	35.6	150.2	176.7	76.8
	10	33.2	3.45	34.9	149.0	176.1	76.5
	20	32.2	3.26	32.9	147.8	175.8	76.4
	40	30.3	3.04	30.7	145.9	176.6	76.7
Simple POM/PCL blend	5	35.1	6.21	45.8	148.5	176.4	78.9
	10	34.4	5.86	43.3	147.6	175.4	78.5
	20	33.0	5.78	42.7	146.3	175.3	78.4
	40	31.5	5.27	38.9	144.4	175.2	78.4

[a] Calculated with eq. (4) for the PCL and POM parts.

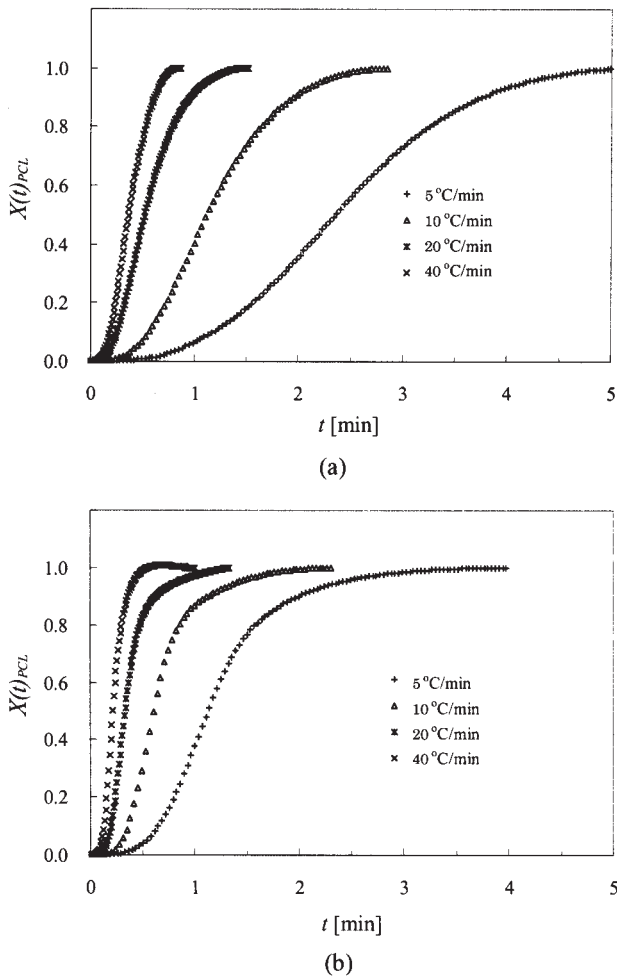

Figure 8 Development of $X(t)_{PCL}$ over time t for nonisothermal crystallization at the indicated cooling rates: (a) reactive POM/PCL blend and (b) simple POM/PCL blend.

than X_{cPCL}, remained nearly constant over the range of the given cooling rates. This indicates that the cooling rate has little effect on X_{cPOM} under these conditions, probably because of the high crystallizability of the POM segments. The reactive blend had a slightly (ca. 2%) lower X_{cPOM} in comparison with the simple blend. The molten PCL part is expected to have high chain mobility when the POM part crystallizes upon cooling and have little influence on X_{cPOM}.

Nonisothermal crystallization kinetic analysis

Nonisothermal crystallization kinetic analysis[21–25] was performed at each cooling rate to investigate the crystallization kinetics of the components in both the reactive POM/PCL blend and the simple POM/PCL blend. Development of the theoretical background of nonisothermal crystallization kinetic analysis was primarily based on Avrami's theory.[26] On the basis of DSC thermograms, the variation of the relative degree of crystallinity was calculated at each cooling rate Φ. The relative degree of crystallinity at arbitrary crystallization temperature T [$X(T)$] is derived from the ratio of the area of the nonisothermal crystallization exotherm, from a start temperature (T_0) up to T, to the total exotherm, from T_0 up to an end temperature (T_∞), with the following equation:

$$X(T) = \frac{\int_{T_0}^{T} [dH(T)/dT]\,dT}{\int_{T_0}^{T_\infty} [dH(T)/dT]\,dT} \tag{5}$$

where $dH(T)/dT$ is the rate of heat evolution at any given temperature. Crystallization time t is related to crystallization temperature T as follows:

$$t = |(T_0 - T)/\Phi| \tag{6}$$

The relative degree of crystallinity as a function of arbitrary crystallization time t [$X(t)$] is converted from eq. (5) and defined as follows:

$$X(t) = \frac{\int_{t_0}^{t} [dH(t)/dt]\,dt}{\int_{t_0}^{t_\infty} [dH(t)/dt]\,dt} \tag{7}$$

where $dH(t)/dt$ is the rate of heat evolution at any given time and t_0 (= 0) and t_∞ are the start time and end time of crystallization, respectively. Figures 8 and 9 show the time dependence of the relative degrees of crystallinity of the PCL and POM components [$X(t)_{PCL}$ and $X(t)_{POM}$, respectively], based on eq. (7), in the reactive blend and the simple blend. Development of $X(t)$ gives a sigmoidal curve for the PCL component (Fig. 8) and an elongated sigmoidal curve for the POM component (Fig. 9).

Under the assumption that crystallization occurs under a constant temperature, the Avrami relationship between $X(t)$ and crystallization time t is adopted to analyze nonisothermal crystallization as follows:[21]

$$1 - X(t) = \exp(-Z_t \times t^n) \tag{8}$$

where Z_t is the rate parameter and n is the Avrami exponent, which describes the nucleation and growth processes in nonisothermal crystallization. Equation (8) is converted to the following equation:

$$\log\{-\ln[1 - X(t)]\} = n \log t + \log Z_t \tag{9}$$

Figures 10 and 11 show the double logarithm plots of $\log\{-\ln[1 - X(t)]\}$ against $\log t$ for the nonisothermal process of the PCL and POM components, respectively, according to eq. (9). The individual curves can be divided into two sections: a primary crystallization process with an initial linear portion and a secondary one with a subsequent tendency to

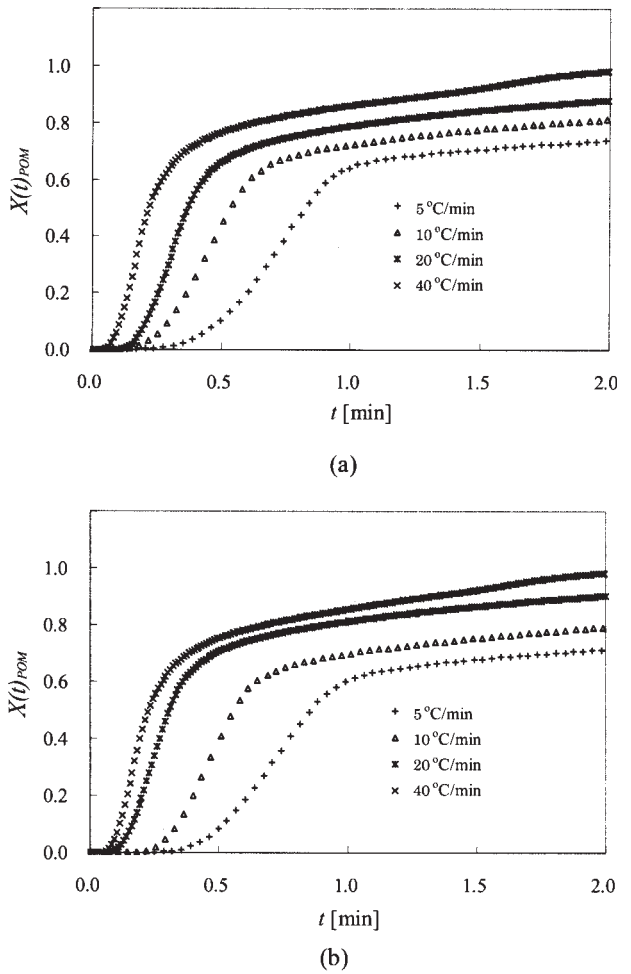

Figure 9 Development of $X(t)_{POM}$ over time t for nonisothermal crystallization at the indicated cooling rates: (a) reactive POM/PCL blend and (b) simple POM/PCL blend.

level off and deviate. Apparently, the plots of $\log\{-\ln[1 - X(t)_{POM}]\}$ versus $\log t$ have a large deviation in Figure 11 when $\log\{-\ln[1 - X(t)_{POM}]\}$ passes zero. Usually, this deviation in the crystallization process is caused by a secondary process of crystallization growth in the later stage, and in many cases, the secondary crystallization process leads to divergence from the Avrami theory.[27] Therefore, only the primary crystallization process is considered in this article. In the primary crystallization, the linear portions shifted to a shorter time as the cooling rate increased. From the slope and intercept of the linear part, $\log\{-\ln[1 - X(t)]\} = -2.3$ to 0 [corresponding to $X(t) = 0.005$ to 0.632], the values of n and the logarithm of the rate parameter ($\log Z_t$) for the PCL and POM parts were determined. The dashed lines in Figures 10 and 11 represent the level of $\log\{-\ln[1 - X(t)]\} = -2.3$ and 0. In general, it must be remembered that in nonisothermal crystallization, the parameter does not have the same physical meaning as in isothermal crystallization. To remove the effect of the cooling rate, the rate parameter characterizing the kinetics of the nonisothermal crystallization (Z_c) is given as follows:[22]

$$\log Z_c = \log Z_t/\Phi \tag{10}$$

The values of n, $\log Z_t$, Z_c, and a correlation coefficient (R^2) for both of the polymer components are listed in Table III.

The Avrami exponent of the PCL part (n_{PCL}) of both of the blends was nearly independent of the cooling rate. In the case of the simple POM/PCL blend, the n_{PCL} values ranged from 3.53 to 3.90. The n_{PCL} values of the reactive POM/PCL blend showed lower values ranging from 2.81 to 2.88, which were always lower than that of the simple blend at any given cooling rate. This suggests that the dimension of crystallization growth of the PCL part was reduced in the confined microphase of the reactive blend and might be mainly dominated by a two-

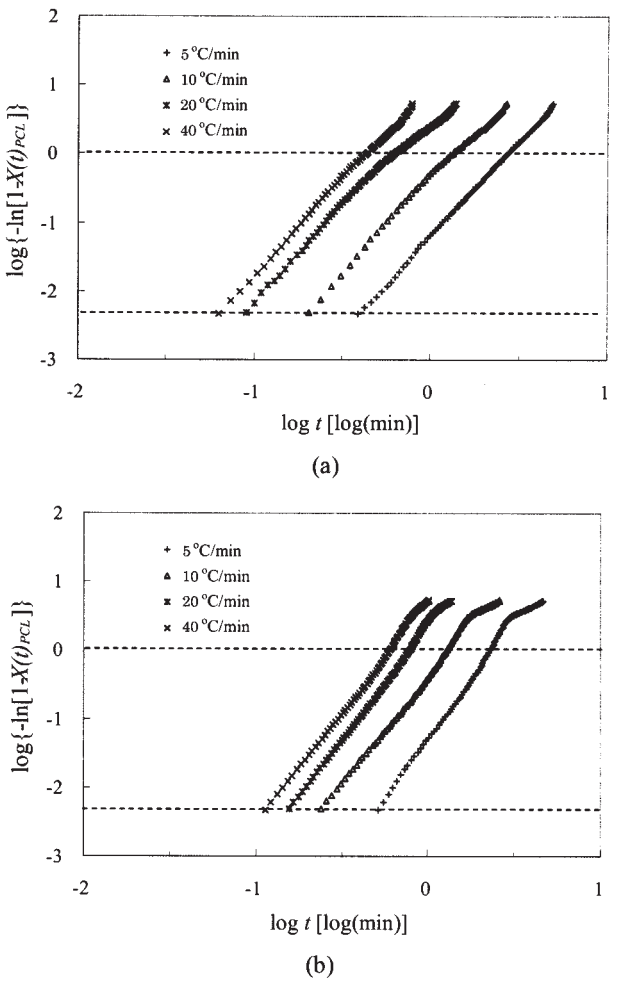

Figure 10 Correlation between $\log\{-\ln[1 - X(t)_{PCL}]\}$ and $\log t$ for nonisothermal crystallization at the indicated cooling rates: (a) reactive POM/PCL blend and (b) simple POM/PCL blend.

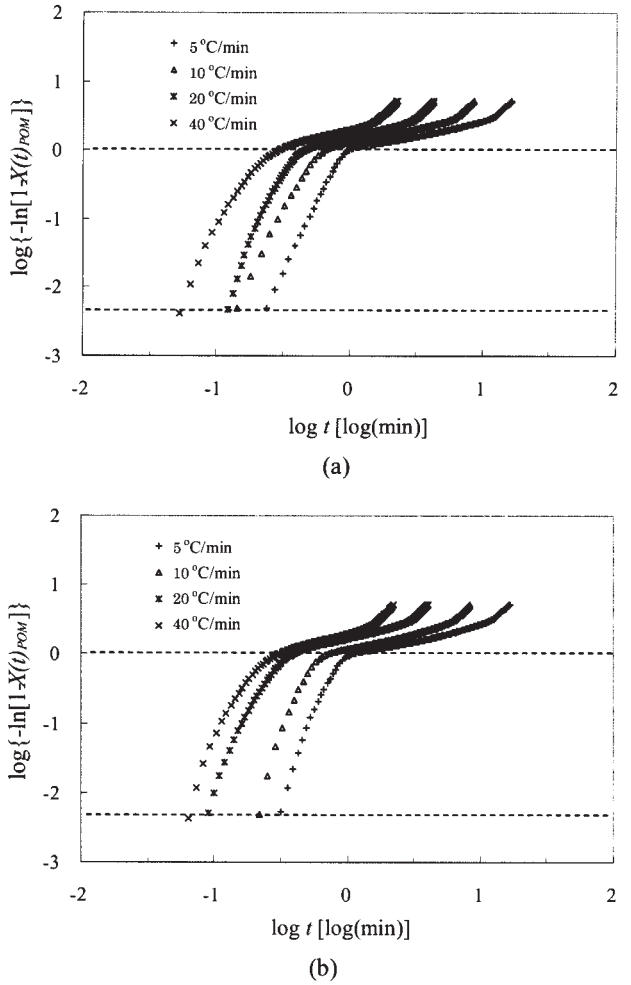

Figure 11 Correlation between $\log\{-\ln[1 - X(t)_{POM}]\}$ and $\log t$ for nonisothermal crystallization at the indicated cooling rates: (a) reactive POM/PCL blend and (b) simple POM/PCL blend.

dimensional mode, that is, a lamellar growth mode in the primary crystallization process. In addition, the crystallization rate parameter of the PCL component (Z_{cPCL}) for the reactive blend was always lower than that of the simple blend. The results are consistent with the fact that the reactive blend had a lower X_{cPCL} value than the simple blend (Table II), indicating that the crystallization rate of the PCL part of the reactive blend was strongly retarded in the primary crystallization process.[10,11] It is reasonable to think that, in the case of the reactive blend, the POM segments crystallize first when the melt is cooling and give a frozen structure, and the crystallization of the PCL part with the covalent bonding to the POM chain is remarkably suppressed and perturbed in the confined microspace.

In contrast to n_{PCL}, the trends of the Avrami exponent of the POM part (n_{POM}) for both of the blends were substantially similar and decreased with an increase in the cooling rate, although n_{POM} showed some scatter, as listed in Table III. The n_{POM} value of the reactive blend and the simple blend ranged from 2.96 to 3.95 and from 3.00 to 4.04, respectively; there was a less significant difference in the variation range of n_{POM}. This indicates that the crystallization mechanism and growth dimension of the POM part in the primary crystallization process for the reactive blend are nearly equal to those for the simple blend. The crystallization rate parameter of the POM component (Z_{cPOM}) also showed no noticeable differences between the reactive blend and the simple blend at the same cooling rate (Table III). This is consistent with the fact that the difference of X_{cPOM} between the two blends was quite small, as listed in Table II. The analytical results can be attributed to the fact that the POM segments have high crystallizability and that the covalent bonds between the POM and PCL parts have little influence on the nonisothermal crystallization kinetic parameters of the POM part in the reactive blend.

CONCLUSIONS

A reactive POM/PCL blend was prepared via cationic bulk polymerization of TOX with DOX in the presence of hydroxyl-terminated PCL as a chain-transfer agent. The morphology and nonisothermal

TABLE III
Parameters of the Nonisothermal Crystallization Kinetics

	Cooling rate (°C/min)	PCL part				POM part			
		n_{PCL}	$\log Z_{tPCL}$	Z_{cPCL}	R^2	n_{POM}	$\log Z_{tPOM}$	Z_{cPOM}	R^2
Reactive POM/PCL blend	5	2.82	−1.202	0.575	0.999	3.95	0.165	1.079	0.996
	10	2.88	−0.286	0.936	0.998	3.50	0.809	1.205	0.988
	20	2.81	0.653	1.078	0.996	3.73	1.475	1.185	0.966
	40	2.88	1.107	1.066	0.999	2.96	1.778	1.108	0.964
Simple POM/PCL blend	5	3.53	−0.337	0.856	0.999	4.02	0.070	1.033	0.961
	10	3.90	0.717	1.180	0.997	4.04	0.837	1.212	0.955
	20	3.88	1.713	1.218	0.997	3.35	1.566	1.198	0.968
	40	3.84	2.402	1.148	0.999	3.00	1.757	1.106	0.948

crystallization of the reactive blend were investigated from the perspective of the mutual influence of two crystallizing parts, and the results were compared with those of the simple POM/PCL blend. TEM observation indicated that the reactive blend had a microscopically phase-separated morphology; the diameter of the PCL microdomain was below 100 nm, which could not be achieved through simple blending. The reactive blend clearly formed ring-banded spherulites, whereas between the two blends, there were no significant differences in the diameters and polygonal edges of spherulites at the same cooling rate. There were also no significant differences between the two blends in the SAXS peaks arising from the long period of POM phases or in the WAXD peaks corresponding to the diffraction with the major POM and minor PCL components. DSC thermograms of the reactive blend showed two crystallization peaks corresponding to the crystallization of the POM and PCL segments. The reactive blend had an approximately 10% lower value of $X_{c\mathrm{PCL}}$ and showed lower n_{PCL} and $Z_{c\mathrm{PCL}}$ values for the PCL part in primary crystallization in comparison with the simple blend. In contrast, $X_{c\mathrm{POM}}$ and the nonisothermal crystallization kinetic parameters of the POM part showed no noticeable differences between the two blends at any given cooling rate. The results will help us to design and optimize modified POMs with desired mechanical properties. On the other hand, it is important to compare the results with those derived for blends having different compositions or molecular weights to further clarify the mutual influence between the two crystallizing parts.

The authors are grateful to Sumika Chemical Analysis Service Co., Ltd., for supporting the transmission electron microscopy observations.

References

1. Masamoto, J.; Yajima, K.; Sakurai, S.; Aida, S.; Ueda, M.; Nomura, S. Polymer 2000, 41, 7283.
2. Matsuzaki, K.; Hata, T.; Sone, T.; Masamoto, J. Bull Chem Soc Jpn 1994, 67, 2560.
3. Radici, P.; Bianchi, G.; Colombo, P. U.S. Pat. 4,160,789 (1979).
4. Radici, P.; Croce, R.; Colombo, P. Ger. Pat. DE 2657965 (1976).
5. Yahiro, S.; Hata, T.; Matsuzaki, K. Jpn. Unexamined Pat. 3-247614 (1991).
6. Nojima, S.; Ono, M.; Ashida, T. Polym J 1992, 24, 1271.
7. Nojima, S.; Akutsu, Y.; Akaba, M.; Tanimoto, S. Polymer 2005, 46, 4060.
8. Kim, J. K.; Park, D. J.; Lee, M. S.; Ihn, K. J. Polymer 2001, 42, 7429.
9. Misra, A.; Garg, S. N. J Polym Sci Part B: Polym Phys 1986, 24, 999.
10. Xu, J. T.; Ding, P. J.; Fu, Z. S.; Fan, Z. Q. Polym Int 2004, 53, 1314.
11. Gan, Z.; Zhang, J.; Jiang, B. J Appl Polym Sci 1997, 63, 1793.
12. Godovsky, Y. K.; Yanul, N. A.; Bessonova, N. P. Colloid Polym Sci 1991, 269, 901.
13. Barker, S. J.; Price, M. B. Polyacetals; Plastics Institute: London, 1970; p 22.
14. Yamashita, Y.; Asakura, T.; Okada, M.; Ito, K. Makromol Chem 1969, 129, 1.
15. Collins, G. L.; Greene, R. K.; Berardinelli, F. M.; Ray, W. H. J Polym Sci Polym Chem Ed 1981, 19, 1597.
16. Kawaguchi, K.; Tajima, Y. Kobunshi Ronbunshu 2005, 62, 124.
17. Lefèvre, C.; Villers, D.; Koch, M. H. J.; David, C. Polymer 2001, 42, 8769.
18. Keith, H. D.; Padden, F. J. Polymer 1984, 25, 28.
19. Starkweather, H. W.; Boyd, R. H. J Phys Chem 1960, 64, 410.
20. Crescenzi, V.; Manzini, G.; Calzolari, G.; Borri, C. Eur Polym J 1972, 8, 449.
21. Mandelkern, L. Crystallization of Polymers; McGraw-Hill: New York, 1964; p 254.
22. Jeziorny, A. Polymer 1978, 19, 1142.
23. Ziabicki, A. Appl Polym Symp 1967, 6, 1.
24. Ozawa, T. Polymer 1971, 12, 150.
25. Nakamura, K.; Katayama, K.; Amano, T. J Appl Polym Sci 1973, 17, 1031.
26. Avrami, M. J Chem Phys 1939, 7, 1103.
27. Xue, M. L.; Yu, Y. L.; Sheng, J.; Chuah, H. H. J Macromol Sci Phys 2005, 44, 531.